High Performance Europium Fluoride Electron-Selective Contacts for Efficient Crystalline Silicon Solar Cells

Linkun Zhang, Lanxiang Meng, Lun Cai, Zhiming Chen, Wenjie Lin, Nuo Chen, Wenxian Wang, Hui Shen, Zongcun Liang*.

Institute for Solar Energy Systems, Guangdong Provincial Key Laboratory of Photovoltaic Technology, School of Physics, Sun Yat-sen University, Guangzhou 510275, China

*Corresponding Author: liangzc@mail.sysu.edu.cn (Prof. Dr. Zongcun Liang).

Abstract

Dopant-free carrier-selective contact has attracted considerable research interests, extensively due to the avoidance of high-temperature doping and its simple, environmental-friendly fabrication processes for crystalline silicon(c-Si) solar cells. In this paper, a novel dopant-free electron-selective material, europium fluoride (EuF_x) has been developed. A desired Ohmic contact can be formed between lightly doped n-type c-Si and aluminum (Al) by inserting nanoscale EuF_x films (2-4 nm) through thermal evaporation so as to avoid the high-temperature phosphorus diffusion and offer a simple, robust process. The contact resistivity is lower than 20 $m\Omega \cdot cm^2$. EuF_x film can effectively select electrons and block holes at the contact interface, which is attributed to its low work function and a large valence band offset with respect to n-type c-Si. Combined with an ultrathin silicon oxide (SiO_2) as a passivation layer, a

This article has been accepted for publication and undergone full peer review but has not been through the copyediting, typesetting, pagination and proofreading process, which may lead to differences between this version and the Version of Record. Please cite this article as doi: 10.1002/solr.202100057.

champion efficiency 21.6% of n-type c-Si solar cells with full-area SiO_2/EuF_x is achieved. An average of absolute efficiency is increased by 12% compared with the reference. The results show that EuF_x has particularly excellent electron-selective transport performance. This work sets up the new possibility of using lanthanide salts as electron-selective contacts for photovoltaic (PV) devices.

1. Introduction

For decades, p-type aluminum back-field (Al-BSF) cells have occupied about 90% of global crystalline silicon (c-Si) solar cells production.[1] However, the direct contact between metal and silicon on the back of cells could introduce large recombination losses resulting in an upper efficiency limit of only ~20% for Al-BSF cell.[2,3] Subsequently, the passivated emitter and rear cell (PERC) had been proposed and gotten development rapidly due to forming local contact on the back to reduce recombination losses significantly and offer commercial cell efficiency in the range 21–24%.[1] In 2013, a n-type Tunnel Oxide Passivated Contact (TOPCon) solar cell was presented by Fraunhofer Institute for Solar Energy Systems, which is compatible with manufacturing process of PERC and upgrade the rear passivation structure. The cell features a random pyramid textured front surface with a boron-diffused emitter, which is passivated by an Al_2O_3/SiN_x antireflection stack. An ultrathin tunnel oxide (SiO_2) and a phosphorus-doped amorphous silicon stack layer are deposited at the rear surface and annealed at high temperature in the range of 800 °C to 900 °C,[4] which act as a passivation layer and electron-selective contact. The full area passivation on the back of TOPCon solar cell can further reduce recombination losses

efficiently, resulted in a higher efficiency enabled cell conversion efficiency exceeding 25%.[5] The use of n-type, rather than p-type c-Si, is desirable because n-type silicon wafers typically exhibit longer carrier lifetimes. This arises primarily due to n-type silicon wafers exclude boron–oxygen complex recombination centers responsible for the light-induced carrier lifetime degradation and exhibit greater tolerance to critical metal impurities.[6,7]

Based on the factors mentioned above, the n-type TOPCon solar cells had been developed rapidly in recent years and could be expected to occupy more market share in the future. However, it is difficult to form Ohmic contact between lightly doped n-type silicon wafer and metal due to the Fermi-level pinning effect, which leads to a relatively high Schottky barrier height (Φ_B) of ≈0.65 eV that hinders the flow of electrons out of the n-type silicon wafer.[8,9] Traditionally, heavy phosphorus doping has been applied under the electrode to mitigate the Schottky barrier,[10] and this approach had gotten great success in producing a large number of industrial silicon solar cells. However, heavy phosphorus doping typically achieved by thermal diffusion involving high-temperature processes greater than 800 °C and also introducing toxic and dangerous sources, which adds manufacturing complexity and safety risks. In recent years, a simpler approach independent of the doping mode was proposed to use dopant-free carrier-elective contact.

Consequently, extensive efforts have been devoted to exploring dopant-free carrier-selective materials to form electron-selective contacts on n-type c-Si wafers without intentional dopants. An alternative approach to reach Ohmic contact on lightly doped n-type crystalline silicon (c-Si) is to deposit thin films with extremely

low work function or suitable band offsets with silicon.[11] Furthermore, these dopant-free carrier-selective contacts that allow low temperature and simple deposition methods (e.g., thermal evaporation, spin-on, and spray methods). Significant progress has been made in the development of dopant-free electron-selective contacts applied to n-type c-Si solar cells. Materials such as alkali/alkaline earth metal salts (e.g., LiF_x,[8,12] CsF,[13] MgF_2[14]), transition metal oxides (TMOs, e.g., TiO_2[15] and TaO_x[16]), alkaline earth metals (e.g., Mg,[17] Ca[18]), alkaline earth metal oxides (e.g., MgO[9]), transition metal nitride and oxynitride (e.g., TaN_x,[11] TiN_x,[19] TiO_xN_y[20]) have been reported to enhance the Ohmic contact of Al to n-type c-Si significantly, enabling the achievement of high efficiency solar cells with most of them reaching about 20%.

In this work, we developed a novel lanthanide salt EuF_x as electron-selective contact for n-type c-Si solar cells. EuF_x was usually studied and applied in the optical fields.[21,22] To our knowledge, the application of EuF_x as electron-selective contacts to n-type c-Si has not been explored. For the first time, this material was applied to the full rear surface of n-type c-Si solar cells as the electron-selective contact in combination with an ultrathin SiO_2 passivation layer, a high efficiency above 21% was achieved without the use of rear heavy n-type doping.

2. Results and Discussion

The composition and chemical states of the elements in EuF_x film were analyzed via X-ray photoelectron spectroscopy (XPS) using monochromatic Al Kα X-rays with a photon energy of 1486.6 eV. The binding energies of all measured data were

calibrated by the surface pollution C 1s (284.8 eV). As shown in Figure 1a, Eu 3d region exhibits complex multiple splitting for Eu (III) compounds.[23] The core level of Eu 3d was assigned to the Eu $3d_{3/2}$ and $3d_{5/2}$. The two small peaks on the right of the main peaks indicate that there are a few Eu^{2+} states in the EuF_x film.[24,25] The peak on the right side of Eu $3d_{3/2}$ in Figure 1a is actually smaller than that on the right side of Eu $3d_{5/2}$. But because the signal strength is so small, that XPSPEAK software can not fit it accurately. While the F 1s spectra exhibits a typical peak at 685.3 eV, visualized in Figure 1b. Extraction of the EuF_x film stoichiometry based on core level peak areas reveals a F to Eu atomic fraction of 2.82, which demonstrates the small amount of F deletion presence in the deposited EuF_x films.

Figure 1c shows the UV photoelectron spectroscopy (UPS) spectrum of EuF_x thin film using a He I excitation (21.22 eV). The work function of EuF_x was measured to be ~3.7 eV. The gap between the Fermi level and the maximum of the valence band ($E_F - E_V$) in EuF_x obtained from the cutoff in the UPS spectrum is ~3.9 eV, leading to a large valence band offset ($\Delta E_v \approx 2.4$ eV) to lightly doped n-Si that can block the holes effectively. This will be discussed in more detail below.

To investigate the electronic contact behavior of the n-type c-Si/EuF_x/Al structure, the contact resistivity ρ_c was measured using the transmission line model (TLM) as shown in Figure 2a.[26] Figure 2b demonstrates the direct contact of n-type c-Si with Al. The sample exhibits a certain extent of Ohmic contact when the pad spacing is small, but then turns to irregular rectifying contact when the pad spacing increases. This non-Ohmic phenomenon between the lightly doped n-type c-Si and Al is due to the presence of a large Schottky barrier at the interface. By inserting the nanoscale

EuF_x film (2-4 nm) between n-type c-Si and Al, the contact behaviors were significantly improved, resulting in perfect Ohmic contact characteristic (linear I–V curve). As shown in Figure 2c, the extracted minimum ρ_c about 15.6 $m\Omega \cdot cm^2$ is obtained from the n-type c-Si/EuF_x/Al contact with 2 nm EuF_x. The low contact resistivity realization is likely attributed to Fermi-level depinning between n-type c-Si and Al.[11] Figure 2d depicts the contact resistivity (ρ_c) as a function of EuF_x thickness. It can be seen that after the EuF_x film was inserted, the ρ_c decrease sharply for the thickness of EuF_x at 2 nm, 2.5 nm, 3 nm, and 4 nm, the contact resistivity is very low (ρ_c<20 $m\Omega \cdot cm^2$), indicating that good Ohmic contact can be formed when the thickness of EuF_x is from 2 nm to 4 nm. The optimal contact resistivity 15.6 $m\Omega \cdot cm^2$ of EuF_x is lower than the minimum contact resistivity 42 $m\Omega \cdot cm^2$ of TaN_x and 20 $m\Omega \cdot cm^2$ of TiO_2 prepared by ALD in the literatures.[11,15] In addition, the lowest ρ_c of EuF_x is lower than 17.5 $m\Omega \cdot cm^2$ of MgO prepared by thermal evaporation in the literature.[9] And it is also lower than the contact resistivity 18.8 $m\Omega \cdot cm^2$ of 2 nm LiF prepared by thermal evaporation in our laboratory (see Figure S1 in the Supporting Information), but higher than the optimal ρ_c value 2 $m\Omega \cdot cm^2$ of LiF reported in the literature.[8] Compared with LiF, EuF_x has the same stability and robustness. LiF has somewhat toxicity that may be harmful to human health and the environment, while EuF_x has no toxicity therefore may have a larger application in silicon solar cells. The contact resistivity achieved by EuF_x is lower than that achieved by MgO, TaN_x and TiO_2, which is most likely due to the fact that EuF_x has a lower work function (3.7 eV) compared to MgO (4.1 eV), TaN_x (4.3 eV) and TiO_2 (>4 eV).[9,11,15] The bands of n-type silicon were induced to bend downward to a greater extent, which is more beneficial to

form an electron aggregation region for electron-selective transporting. This will be further explained below. These results reflect that EuF_x can be acted as an excellent electron-selective contact material, which gives us a possibility of preparing full-area electron-selective contact for high-efficiency silicon cells in combination with a passivation layer, such as amorphous silicon or SiO_2.[14, 15, 20, 27-31] We prepared n-type c-Si solar cells using SiO_2 as the passivation layer and 2-4 nm EuF_x as the electron-selective material to achieve more than 20% efficiencies, and the following part will describe in detail. We also measured the contact resistivity between EuF_x and n-type silicon covered by SiO_2, and the results were less than 50 $m\Omega \cdot cm^2$. We must point out that the extracted ρ_c value were measured by the two-probe method and can be considered as the upper limit ρ_c at the EuF_x/n-Si heterocontact.

To investigate the structure and composition of the EuF_x based electron contact. The n-type c-Si/EuF_x (4 nm)/Al (20 nm)/Ag (as a shield) stack was fabricated, and scanning transmission electron microscopy (STEM) imaging coupled to energy-dispersive X-ray spectroscopy (EDX) were performed. Figure 4a displays a high angle annular dark-field (HAADF) STEM interface imagine with a resolution of 30 nm, which visualizes an obvious EuF_x interlayer. Figure 4b provides an accompanying mapping of the local Si, Eu, F, Al, and Ag EDX signals at the same resolution. It can be observed clearly that a uniform Eu and F elemental distributions across the interface without intermixing of the Al and Si layers. Figure 4c presents a high-resolution of 5 nm STEM cross-sectional imaging. Crystalline silicon substrate and EuF_x thin film can be distinctly identified, revealing that the 4 nm thermally evaporated EuF_x layer between the silicon and Al is homogeneous and continuous,

and the thickness of the film is very accurate according to the measurement result (~4.02 nm).

To further testify the performance of EuF_x/Al electron-selective contact on the devices, we fabricated n-type silicon solar cells (2×2 cm^2) featuring full-area SiO_2/EuF_x/Al/Ag stack, where SiO_2 was used as the passivation layer, EuF_x/Al was the electron-selective contact, and Ag acts as a thickening electrode. Figure 3a presents a schematic of the cell structure. The front surface of the cell features a textured structure with random pyramids for light trapping to enhance light absorption. And then boron diffused forms a p^+ region to collect holes, which was passivated by Al_2O_3 and then coated with SiN_x antireflection layer. The rear side features an ultrathin SiO_2 (~1.7 nm) passivation layer, capped with the full-area thermally evaporated EuF_x/Al/Ag stack. Compared with conventional silicon cells of heavily doped contact, the EuF_x based electron-selective contact avoids the phosphorus diffusion process at high temperature and allows a low complexity fabrication to realize the electrons transfer to the rear electrode. A reference cell without EuF_x interlayer at the rear side was fabricated for comparison.

The illuminated current density–voltage (*J*–*V*) characteristics of silicon solar cells with and without EuF_x rear contact structures under one sun standard illumination are shown in Figure 3b. In addition, we also examined the effect of EuF_x thicknesses on cell performance. The detailed photovoltaic parameters can be seen in Table 1. It can be seen from Table 1 that adequate EuF_x thickness (2-4 nm) can result in Ohmic contact, combined with a passivation layer of SiO_2 enabled the demonstration of exceeding 20%-efficiency cells, highlighting that EuF_x is an excellent

electron-selective contact for c-Si solar cells. And as the thickness of EuF_x increases from 2 nm to 4 nm, the cell efficiency increases gradually from 20.3% to 21.6%. We believe that the small improvement in cell efficiency may be determined by the film formation status of EuF_x films. The continuity of EuF_x film with a thickness of 2 nm may not be good enough. With the gradual increase of film thickness, the film's uniformity and continuity may become better, and thus the electron-selective performance will be better. Notably, the insertion of a 4 nm EuF_x film drastically improves all the parameters of the solar cell, leading to a champion efficiency of 21.6%, associated with an open-circuit voltage (V_{oc}), short-circuit current density (J_{sc}), and fill factor (FF) of 662.8 mV, 40.43 mA cm^{-2}, and 80.46%, respectively. Compared to the reference cell without EuF_x, both V_{oc} and FF were significantly improved, from 349.0 mV to 662.8 mV and from 70.99% to 80.46%, respectively, which resulted in an average 12% absolute efficiency improvement. The increase of the FF and V_{oc} can be most likely due to the suppression of non-Ohmic contact phenomena result from a dramatic decrease of the rear contact resistance, visualized in Figure 2, and the good passivation effect of SiO_2. Although the reference cell also has a passivation layer of SiO_2, however, the rear surface is non-Ohmic contact, which would hinder carrier collection, indicating that only under the condition of Ohmic contact, good passivation could be the key to realize high efficiency solar cells. Compared to other electron-selective materials used as electron transport layer on the n-type silicon solar cells covered with a passivation layer, the champion efficiency of EuF_x is higher than 20.6% achieved by LiF in the literature.[8] Compared with the champion efficiency of 21.6% achieved by TiO_2 on the n-type solar cell that

also used SiO_2 as a passivation layer in the literature,[15] the obtained highest efficiency by applying EuF_x on the back of solar cell is the same as that achieved by TiO_2. However, the cell applied TiO_2 had been treated by forming gas atmosphere (FGA) annealing, while EuF_x was prepared only by a simple thermal evaporation. FGA annealing can improve the chemical passivation effect of SiO_2 and the FF of the solar cell.[15] Therefore, the contrast above illustrates that EuF_x has excellent electron-selective performance. It may be doubtful why there is such a large absolute efficiency improvement, relative to MgO_x 5%,[9] TaN_x 4%.[11] We believe that the low efficiency of the reference cells is the reason for such a big improvement. Lightly doped n-type c-Si direct contact with Al exhibits non-Ohmic contact behavior couple with an insulating SiO_2 layer, resulting in electron transmission on the back of the cell further hampered, so that the efficiency is unusually low only about 9%. This, in turn, further confirms the strong electron selectivity of EuF_x. Without heavy doping, the good charge carrier transport can be realized, enabling electrons tunneling through the SiO_2 passivation insulation layer. Figure 3c shows the external quantum efficiency spectral response of the cells, with and without EuF_x interlayer, respectively. It can be seen that both devices present particularly high quantum efficiency at the short wavelength range (lower than ~700 nm), which were attributed to the high-quality passivation and antireflection performance in the front side of the cells provided by Al_2O_3 and SiN_x stack. During the long wavelength range, the EQE of devices with EuF_x improved dramatically in comparison to that without EuF_x. This is due to the remarkable passivation effect of SiO_2 on the condition that EuF_x achieves perfect Ohmic contact.

In order to clarify the carriers transport mechanism on the back of the n-type c-Si solar cells, the band alignment was studied, and the band diagrams were presented in Figure 4. As shown in Figure 4a, the n-type c-Si is in direct contact with Al, which exists Fermi-level pinning phenomenon, exhibits a large Schottky barrier as mentioned above, hampering the flow of electrons out of the n-type silicon. Figure 4b illustrates the contact between n-type c-Si and EuF_x with an ultrathin SiO_2 interlayer. The optical band gap of EuF_x is about 4.1 eV, which was obtained by the calculation of the EuF_x thin film's transmittance measured by a UV-vis-NIR spectrophotometer (see Figure S2, Supporting Information). The gap between the Fermi level and the maximum of the valence band ($E_F - E_V$), visualized in Figure 1c, is ~3.9 eV. The gap between the Fermi level and the maximum of the valence band of the n-type c-Si substrate is ~0.9 eV obtained from the valence band spectrum in the XPS measurement (see Figure S3, Supporting Information). EuF_x has a low work function. When it contacts with n-type c-Si, electrons flow to silicon, and the bands of silicon are induced to bend down to form an electron accumulation region at the surface of n-type c-Si. Such a n^+ region thus acts as the electron-selective contact in this type solar cells.[32] Even though there is a barrier that the insulating SiO_2 layer brings, electrons can tunnel and pass through the EuF_x layer effectively. [33] On the other hand, there exists a large valence band offset ($\Delta E_v \approx 2.4$ eV) that can block the holes notably. The results further elucidate that EuF_x is an excellent electron-selective contact for n-type c-Si, which is consistent with the experimental results in Figure 2c and Figure 3c. Figure 4c visually depicts the contact between the n-type c-Si covered with a SiO_2 passivation layer and Al. Because the n-type c-Si contact with Al

exhibiting a large Schottky barrier couple with the barrier of SiO_2 insulation layer, electrons are hard to pass through, which is accounted for the demonstration of a particularly low cell efficiency presented in Figure 3c.

3. Conclusion

We have demonstrated a novel dopant-free EuF_x/Al electron-selective contact for silicon solar cells deposited at a low temperature and without the use of heavy n-type doping. The obtained optimal contact resistivity of the EuF_x/Al contact (~15 $m\Omega \cdot cm^2$) presented a perfect Ohmic contact on lightly doped n-type silicon, suggesting that EuF_x is an excellent electron-selective contact for c-Si heterojunctions. The n-type silicon solar cells featuring an ultrathin SiO_2 passivation layer and full-area EuF_x/Al electron-selective contact on the rear side achieved the PCE of exceeding 20%, and the champion efficiency is 21.6%. The novel EuF_x electron-selective material together with its low level of complexity deposition techniques may promise a prospective future for high efficiency, low temperature, dopant-free silicon solar cells.

4. Experimental section

EuF_x thin films were thermally evaporated at a rate of 0.2 Å/s from high purity (>99.99%) stoichiometric EuF_3 sources in a vacuum chamber with a base pressure $<5 \times 10^{-4}$ Pa. For XPS and UPS characterization analysis, samples were fabricated on single-side mechanically polished, Czochralski (Cz) c-Si wafers. The chemical components and bonding states of EuF_x film were detected via high-resolution X-ray photoelectron spectroscopy (ESCALAB 250, Thermo Fisher Scientific) equipped

with a monochromatic Al *K*α X-ray source (1486.6 eV) in an ultrahigh vacuum chamber with a base pressure of 2×10^{-9} mbar. The work function measurements of the EuF_x were determined by UV photoelectron spectroscopy (ESCALAB 250, Thermo Fisher Scientific) using a He-I excitation (21.22 eV) at a base pressure 5×10^{-10} mbar. To observe the low energy secondary electron cut-off, a bias voltage of -5V was added to the sample. The final output UPS data has been subtracted by the added bias.

Contact resistivity test structures were performed on a series of Cz n-type c-Si wafers with a resistivity in the 1-3Ω·cm range. The silicon wafers were subjected to a KOH solution (20 vol%) heated at a temperature of 85 °C for 13 min to remove the surface damage. All samples were then cleaned by the Radio Corporation of America (RCA) procedure, leading to a thickness of 170 μm. TLM pads composed of a stack of EuF_x with a variety of thicknesses capped with ~20 nm Al and ~300 nm Ag (the silver acts as a thickening electrode) were deposited via a shadow mask. The specific contact resistivity was extracted with the dark current-voltage (I-V) measurement at room temperature using a Keithley 2400 source meter.

To further investigate the EuF_x based electron-selective contact structure, EuF_x (4 nm)/Al (20 nm)/Ag (500 nm) stack was evaporated on a single-side mechanically polished Cz c-Si wafer. The cross-sectional analysis was prepared using the focused ion beam (FIB) lift-out technique by a Helios 450S Dual Beam FIB system. Following, STEM HAADF images coupled to EDX were obtained using a FEI TitanThemis 200 TEM system operated at 200 kV.

Proof-of-concept cells were fabricated on lightly doped Cz n-type c-Si wafers with a resistivity of 1 Ω·cm. The wafers were textured with random pyramids in a KOH solution. After RCA cleaning, the boron emitter was formed in a boron diffusion furnace using a BBr_3 source. The front boron diffused textured surfaces were then passivated with a ~10 nm atomic layer deposited (ALD) Al_2O_3 and ~80 nm plasma enhanced chemical vapor deposited (PECVD) SiN_x antireflection stack. A tunneling SiO_x is thermally grown on the undiffused rear silicon surfaces in a low-pressure chemical vapor deposition (LPCVD) system. The front metal electrodes were prepared by screen printing and then sintered at 750 ℃. The rear contact was formed by thermally evaporating a stack of EuF_x with a variety of thicknesses capped with ~20 nm Al and ~500 nm Ag. The light *J*–*V* behavior was measured under standard one sun conditions (100 mW cm^{-2}, AM1.5 spectrum, 25 °C) using a VS-6821 M Solar Cell I-V Tester. The tester was calibrated with a certified Fraunhofer reference cell. The external quantum efficiency (EQE) was attained using a solar cell quantum efficiency measurement system (Enlitech QE-R). The optical properties of the EuF_x films deposited on glass were measured using a UV-vis-NIR spectrophotometer (U-4100 from Hitachi).

Acknowledgements

This work was supported by the National Natural Science Foundation of China (Grant No. 61774173).

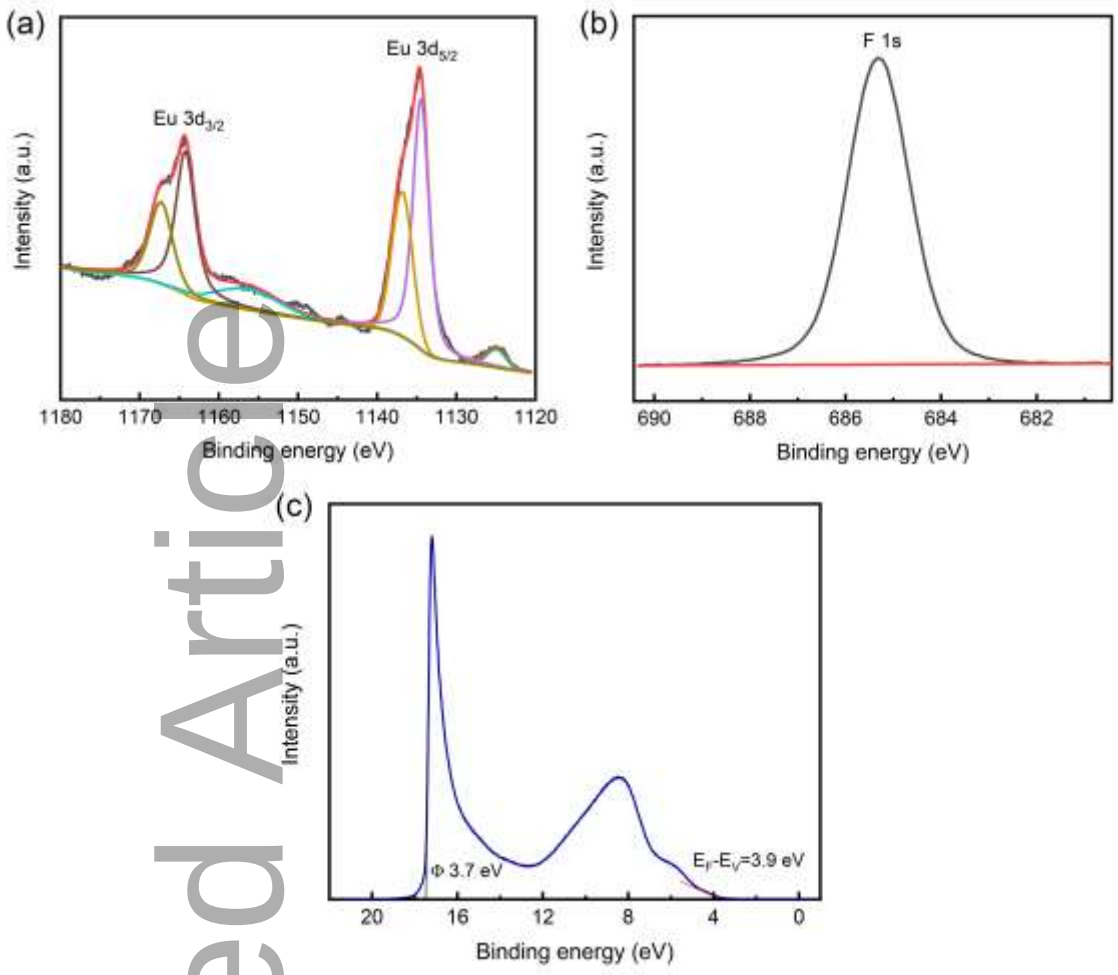

Figure 1. XPS and UPS measurements of thermally evaporated EuF_x films. a) The core level spectrum of Eu 3d. b) The core level spectrum of F 1s. c) The UPS spectrum of EuF_x film.

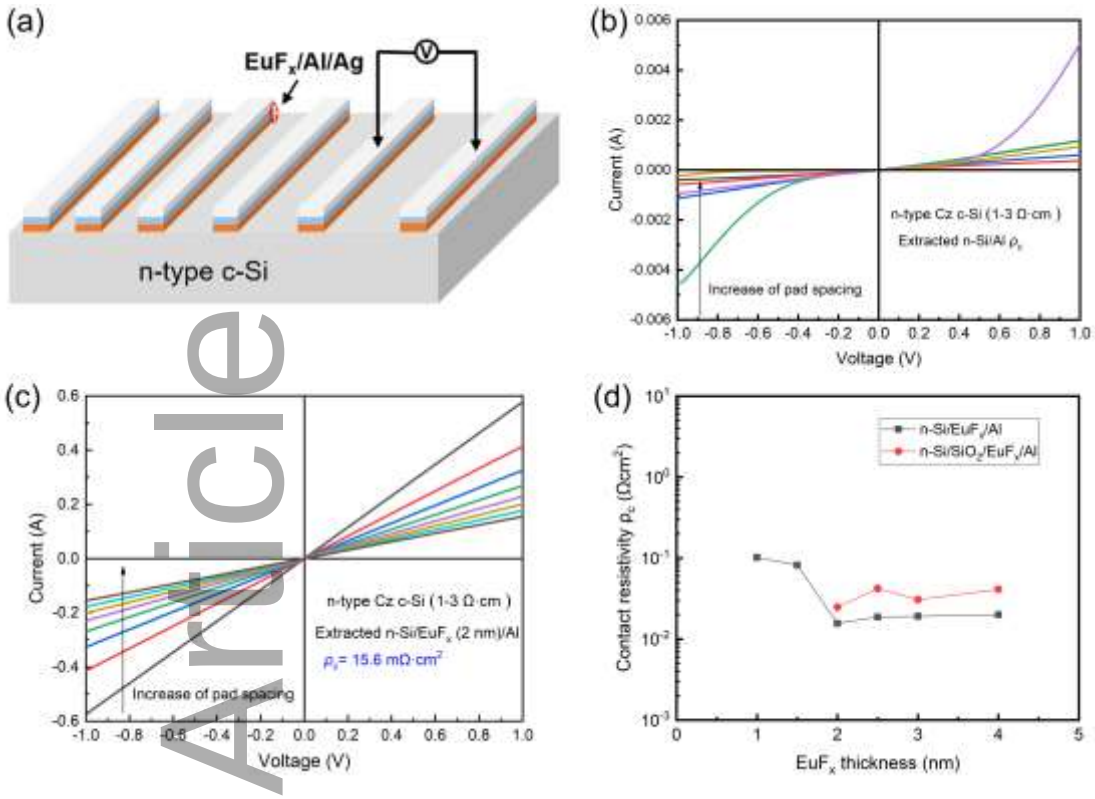

Figure 2. Contact resistivity measurements of EuF_x based contacts to n-type c-Si. a) Schematic of the TLM test structure. b, c) Dark *I–V* measurement results of samples without and with 2 nm EuF_x interlayer between Al and n-type c-Si, respectively. d) The contact resistivity ρ_c with and without a SiO_2 passivation layer as a function of EuF_x thickness.

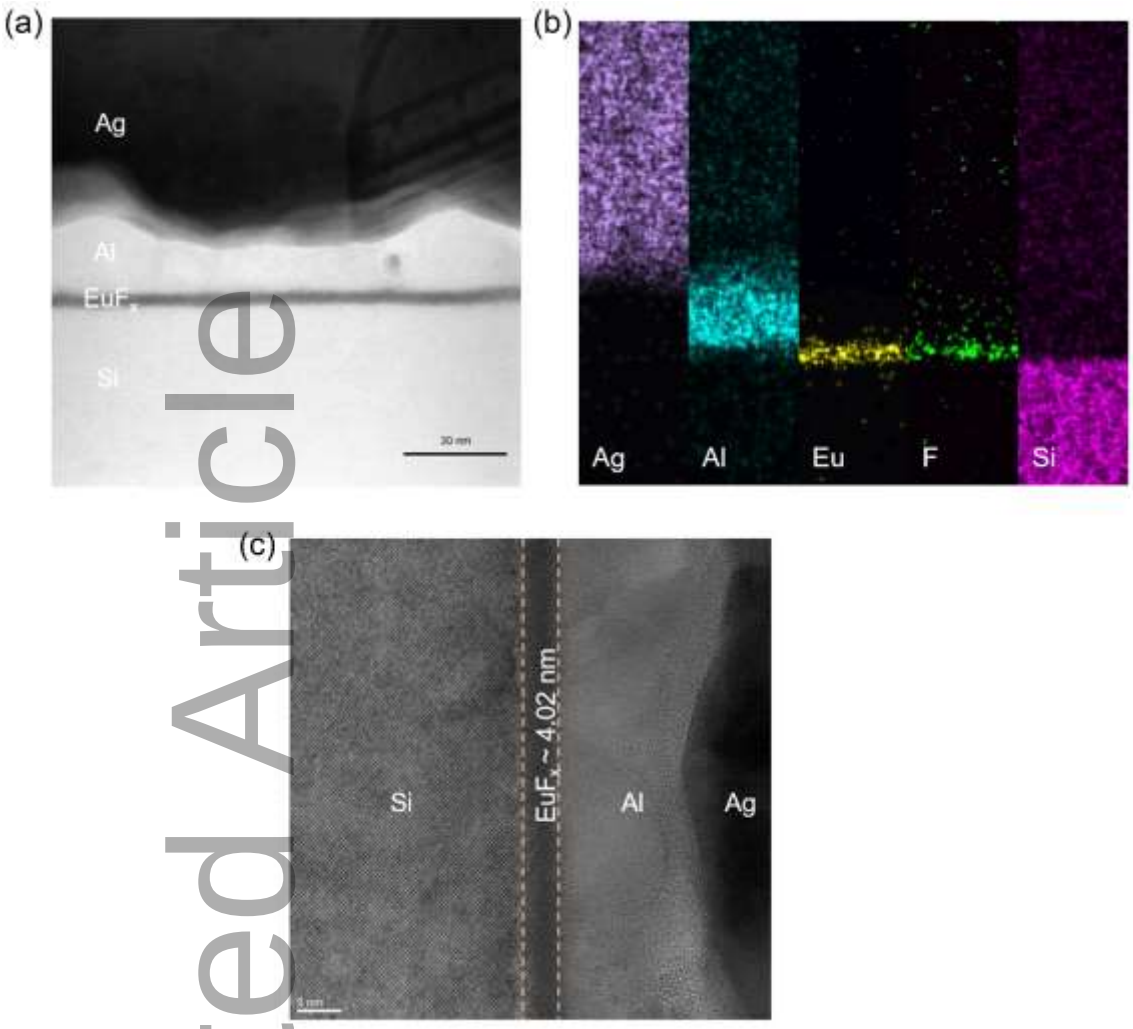

Figure 3. STEM measurements of the c-Si/EuF_x (4 nm)/Al (20 nm)/Ag contact structure's cross-section. a) STEM HAADF microscopy image of the c-Si/EuF_x/Al/Ag contact. b) EDX mapping of Ag, Al, Eu, F, and Si signals at the same resolution as a). c) High-resolution STEM HAADF microscopy image of the c-Si/EuF_x/Al/Ag contact.

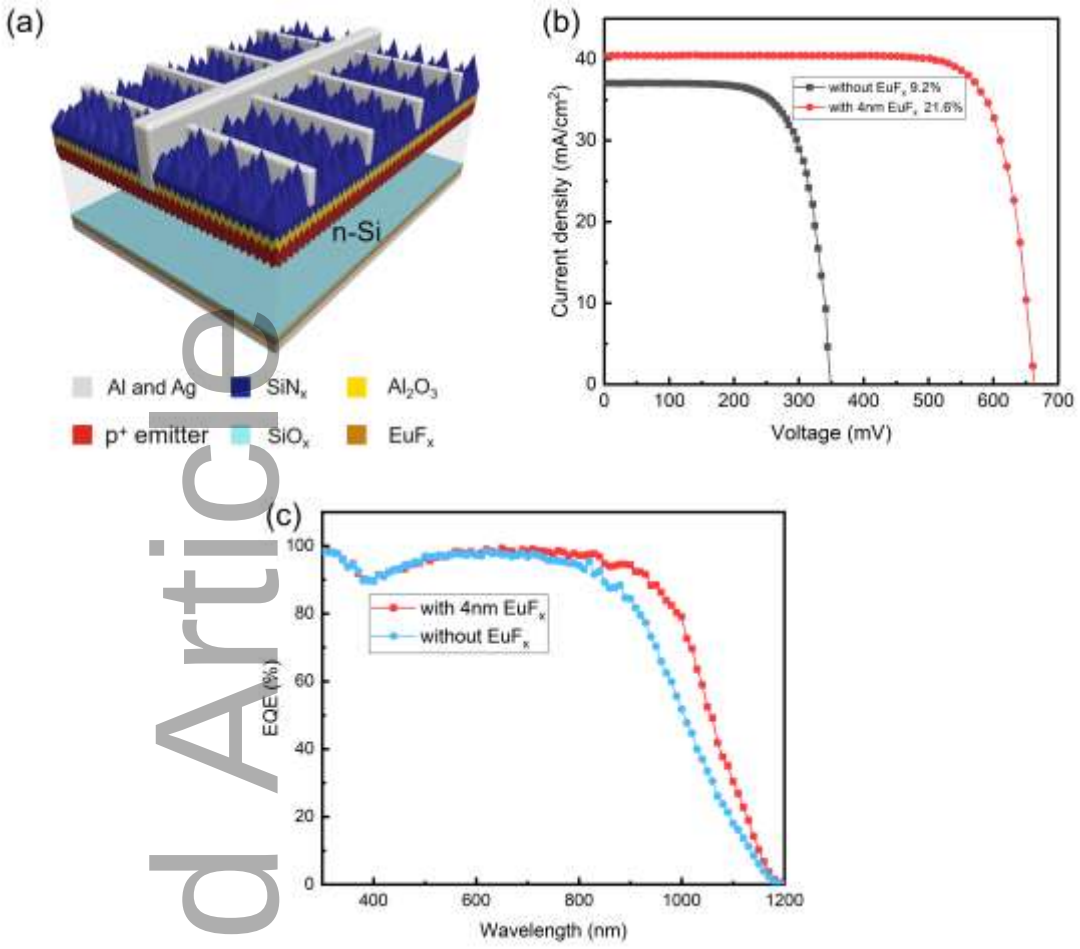

Figure 4. Device results covered with full-area rear SiO_2 passivation layer and EuF_x based electron-selective contacts. a) The schematic of n-type c-Si solar cell featuring full-area rear SiO_2/EuF_x/Al /Ag stack. b) The illuminated $J - V$ curves and PCE for cells without and with ≈4 nm EuF_x interlayer. c) External quantum efficiency of the cells with and without a EuF_x interlayer.

Table 1. Photovoltaic parameters of n-type c-Si solar cells without or with a full area EuF_x-based electron-selective contact.

EuF_x thickness	V_{oc} (mV)	J_{sc} (mA cm^{-2})	*FF* (%)	η (%)
0 nm	349.0	37.04	70.99	9.2
2 nm	649.6	38.60	80.93	20.3
3 nm	657.9	39.86	79.53	20.9
4 nm	662.8	40.43	80.46	21.6

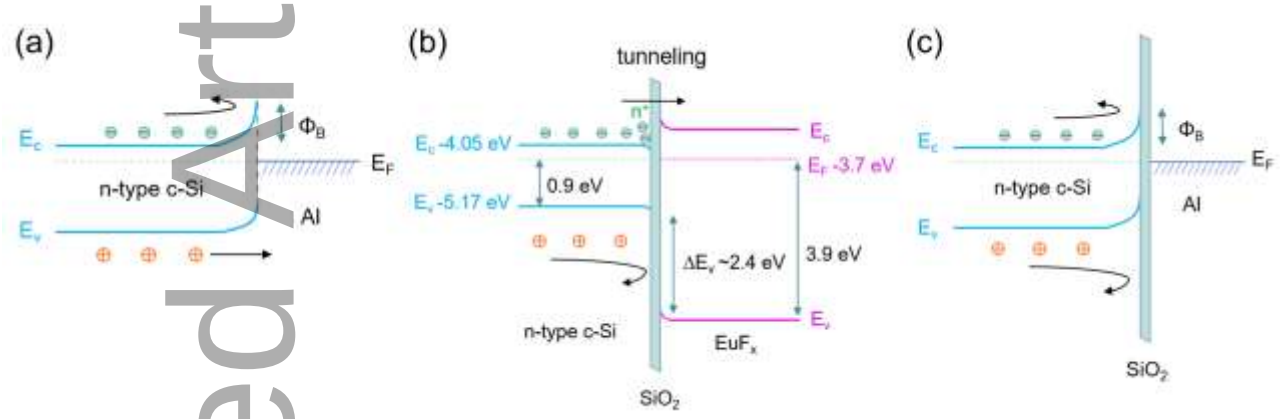

Figure 5. Band alignments of the n-type c-Si solar cells with different rear contacts. a) Band alignment at lightly doped n-Si/Al interface. b) Band alignment between the lightly doped n-Si and EuF_x inserted with an ultrathin SiO_2. c) Band alignment between the lightly doped n-Si and Al inserted with an ultrathin SiO_2.

Reference

[1] A. Blakers, IEEE J. Photovoltaics 2019, 9, 629.

[2] F. Fertig, R. Lantzsch, A. Mohr, M. Schaper, M. Bartzsch, D. Wissen, F. Kersten, A. Mette, S. Peters, A. Eidner, J. Cieslak, K. Duncker, M. Junghänel, E. Jarzembowski, M. Kauert, B. Faulwetter-Quandt, D. Meißner, B. Reiche, S. Geißler, S. Hörnlein, C. Klenke, L. Niebergall, A. Schönmann, A. Weihrauch, F. Stenzel, A. Hofmann, T. Rudolph, A. Schwabedissen, M. Gundermann, M. Fischer, J. W. Müller, D. J. W. Jeong, Energy Procedia 2017, 124, 338.

[3] T. Fellmeth, S. Mack, J. Bartsch, D. Erath, U. Jäger, R. Preu, F. Clement, D. Biro, IEEE Electron Device Letters 2011, 32, 1101.
[4] F. Feldmann, M. Bivour, C. Reichel, H. Steinkemper, M. Hermle, S. W. Glunz, Sol. Energy Mater. Sol. Cells 2014, 131, 46.
[5] A. Richter, J. Benick, F. Feldmann, A. Fell, M. Hermle, S. W. Glunz, Sol. Energy Mater. Sol. Cells 2017, 173, 96.
[6] J. Schmidt, A. Cuevas, J. Appl. Phys. 1999, 86, 3175.
[7] D. Macdonald, L. J. Geerligs, Appl. Phys. Lett. 2004, 85, 4061.
[8] J. Bullock, P. Zheng, Q. Jeangros, M. Tosun, M. Hettick, C. M. Sutter-Fella, Y. Wan, T. Allen, D. Yan, D. Macdonald, S. De Wolf, A. Hessler-Wyser, A. Cuevas, A. Javey, Adv. Energy Mater. 2016, 6.
[9] Y. Wan, C. Samundsett, J. Bullock, M. Hettick, T. Allen, D. Yan, J. Peng, Y. Wu, J. Cui, A. Javey, A. Cuevas, Adv. Energy Mater. 2017, 7.
[10] J. Benick, B. Hoex, M. C. M. van de Sanden, W. M. M. Kessels, O. Schultz, S. W. Glunz, Appl. Phys. Lett. 2008, 92.
[11] X. Yang, E. Aydin, H. Xu, J. Kang, M. Hedhili, W. Liu, Y. Wan, J. Peng, C. Samundsett, A. Cuevas, S. De Wolf, Adv. Energy Mater. 2018, 8.
[12] J. Bullock, M. Hettick, J. Geissbühler, A. J. Ong, T. Allen, Carolin M. Sutter-Fella, T. Chen, H. Ota, E. W. Schaler, S. De Wolf, C. Ballif, A. Cuevas, A. Javey, Nat. Energy 2016, 1.
[13] W. Wang, J. He, L. Cai, Z. Wang, S. K. Karuturi, P. Gao, W. Shen, Sol. RRL 2020, 4.
[14] Y. Wan, C. Samundsett, J. Bullock, T. Allen, M. Hettick, D. Yan, P. Zheng, X. Zhang, J. Cui, J. McKeon, A. Javey, A. Cuevas, ACS Appl. Mater. Interfaces 2016, 8, 14671.
[15] X. Yang, Q. Bi, H. Ali, K. Davis, W. V. Schoenfeld, K. Weber, Adv. Mater 2016, 28, 5891.
[16] Y. Wan, S. K. Karuturi, C. Samundsett, J. Bullock, M. Hettick, D. Yan, J. Peng, P. R. Narangari, S. Mokkapati, H. H. Tan, C. Jagadish, A. Javey, A. Cuevas, ACS Energy Lett. 2017, 3, 125.
[17] Y. Wan, C. Samundsett, D. Yan, T. Allen, J. Peng, J. Cui, X. Zhang, J. Bullock, A. Cuevas, Appl. Phys. Lett. 2016, 109.
[18] T. G. Allen, J. Bullock, P. T. Zheng, B. Vaughan, M. Barr, Y. M. Wan, C. Samundsett, D. Walter, A. Javey, A. Cuevas, Prog. Photovoltaics Res. Appl. 2017, 25, 636.
[19] X. Yang, W. Liu, M. De Bastiani, T. Allen, J. Kang, H. Xu, E. Aydin, L. Xu, Q. Bi, H. Dang, E. AlHabshi, K. Kotsovos, A. AlSaggaf, I. Gereige, Y. Wan, J. Peng, C. Samundsett, A. Cuevas, S. De Wolf, Joule 2019, 3, 1314.
[20] X. Yang, Y. Lin, J. Liu, W. Liu, Q. Bi, X. Song, J. Kang, F. Xu, L. Xu, M. N. Hedhili, D. Baran, X. Zhang, T. D. Anthopoulos, S. De Wolf, Adv. Mater. 2020, 32, e2002608.
[21] H. H. Caspers, H. E. Rast, J. L. Fry, J. Chem. Phys. 1967, 47, 4505.
[22] Q.-L. H. Miao Wang, Jian-Ming Hong, Xue-Tai Chen,and Zi-Ling Xue, Cryst. Growth Des. 2006, 6, 1972.
[23] F. Mercier, C. Alliot, L. Bion, N. Thromat, P. Toulhoat, J. Electron. Spectrosc. Relat. Phenom 2006, 150, 21.
[24] D. Kim, Y. H. Jin, K. W. Jeon, S. Kim, S. J. Kim, O. H. Han, D. K. Seo, J. C. Park, Rsc Advances 2015, 5, 74790.
[25] D. Kim, S. C. Kim, J. S. Bae, S. Kim, S. J. Kim, J. C. Park, Inorg Chem 2016, 55, 8359.
[26] G. K. Reeves, H. B. Harrison, IEEE Electron Device Lett. 1982, 3, 111.
[27] F. Feldmann, M. Bivour, C. Reichel, M. Hermle, S. W. Glunz, Sol. Energy Mater. Sol. Cells 2014, 120, 270.
[28] D. Chen, Y. Chen, Z. Wang, J. Gong, C. Liu, Y. Zou, Y. He, Y. Wang, L. Yuan, W. Lin, R. Xia, L. Yin, X. Zhang, G. Xu, Y. Yang, H. Shen, Z. Feng, P. P. Altermatt, P. J. Verlinden, Sol. Energy Mater. Sol. Cells 2020, 206.
[29] J. He, W. Wang, L. Cai, H. Lin, Z. Wang, S. K. Karuturi, P. Gao, Adv. Funct. Mater. 2020, 30.
[30] K. Yoshikawa, H. Kawasaki, W. Yoshida, T. Irie, K. Konishi, K. Nakano, T. Uto, D. Adachi, M. Kanematsu, H. Uzu, K. Yamamoto, Nat. Energy 2017, 2.
[31] K. Yoshikawa, W. Yoshida, T. Irie, H. Kawasaki, K. Konishi, H. Ishibashi, T. Asatani, D. Adachi, M. Kanematsu, H. Uzu, K. Yamamoto, Sol. Energy Mater. Sol. Cells 2017, 173, 37.
[32] L. G. Gerling, C. Voz, R. Alcubilla, J. Puigdollers, J. Mater. Res. 2016, 32, 260.

[33] R. Garcia-Hernansanz, E. Garcia-Hemme, D. Montero, J. Olea, A. del Prado, I. Martil, C. Voz, L. G. Gerling, J. Puigdollers, R. Alcubilla, Sol. Energy Mater. Sol. Cells 2018, 185, 61.

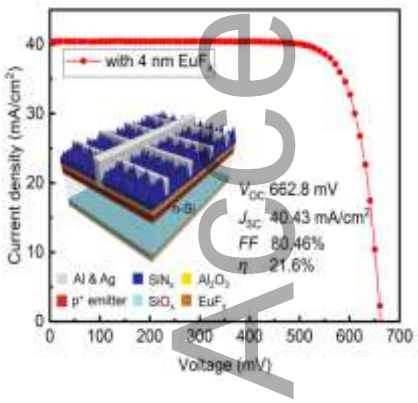

EuF$_x$ is an excellent electron-selective material. A desired Ohmic contact can be formed between lightly doped n-type c-Si and Al by inserting 2-4 nm EuF$_x$ films. The

contact resistivity is lower than 20 $m\Omega \cdot cm^2$. Combined with an ultrathin SiO_2 as a passivation layer, a champion efficiency 21.6% of n-type c-Si solar cells with full-area SiO_2/EuF_x is achieved.